JOURNAL OF CATALYSIS 138, 129–144 (1992)

# An Activation–Deactivation Model for Catalytic Deposition of Carbon

P. McALLISTER[1] AND E. E. WOLF[2]

*Department of Chemical Engineering, The University of Notre Dame, Notre Dame, Indiana 46556*

Received November 1, 1991; revised May 26, 1992

A sequence of reaction steps that corresponded to the fundamental phenomena of adsorption/desorption of a hydrocarbon and hydrogen, hydrogenation/dehydrogenation surface reactions, carbon diffusion and precipitation, catalytic site activation, and deactivation involved in catalytic deposition of carbon from hydrocarbons is proposed. Rate expressions derived from the reaction sequence yielded a kinetic model for simultaneous carbon deposition, catalytic site activation, and catalyst deactivation, which exhibited trends qualitatively similar to experimental results for Ni-catalyzed carbon deposition from propylene/hydrogen mixtures. It was found that increasing the $H_2$ concentration decreased the rates of deposition and poisoning but did not affect the rate of site activation. Thus, higher $H_2$ concentrations lead to lower initial deposition rates, but the total level of deposition increases because of reduced deactivation rates. The hydrocarbon concentration affected the rates of activation, poisoning, and deposition similarly so that the ultimate level of deposition was independent of the hydrocarbon concentration. However, as the hydrocarbon concentration increased, the time over which deposition occurred decreased due to an increased rate of deactivation. Optimized fits of the model to experimental data at various temperatures showed that the model agreed well with data at $H_2$ concentrations from 0.0 to 45%, propylene concentrations up to 3%, and temperatures up to 550°C. 

## 1. INTRODUCTION

The experimental results reported by McAllister and Wolf (*1*) for catalytic carbon deposition on carbon fiber-supported Ni catalysts from $C_3H_6/H_2$ gas mixtures exhibited an interesting time-dependent behavior. In the initial stages of catalytic carbon deposition, an activation period occurred in which the rate of deposition increased significantly. Following the activation stage, the deposition rate decreased as catalyst deactivation became dominant over activation processes. Similar findings of activation–deactivation in the catalytic formation of carbon filaments have been reported by several researchers (*2–13*) for carbon deposition from hydrocarbons on various catalysts and in a variety of other systems as well. Some examples include polymerization reactions of benzyl alcohol (*14*) and ethylene (*15*), dehydrogenation of isopropanol (*16*), hydrogenation of CO (*17, 18*) and benzene (*19*), Fischer Tropsch synthesis (*20–24*), carbon dioxide methanation (*25*), Kölbel–Engelhardt synthesis (*26*), CO oxidation (*27*), hydrodesulfurization (*28*), hydrodechlorination (*29*), and isomerization of *n*-butane (*30*). Activation–deactivation behavior has been observed on a wide range of catalysts including $SiO_2$, $Al_2O_3$, Fe, Cr, Cu, Ni, Pd, Rh, Pt, $CeCu_2$, $NdCu_2$, Co, and $AlCl_3$. The reported causes of the activation behavior include oxidation and reduction effects during reaction (*15, 16, 18, 23, 24, 26, 31*), increases in active surface area (*1, 20*), creation of surface defects (*25*), and formation of active surface carbon (*23, 24*).

Since catalyst deactivation is an extremely important consideration in many processes, many authors have proposed models for deactivation and Forzatti *et al.* (*32*) have reviewed some of these. The early rate expressions for deactivation were em-

[1] Present address: Shell Development Company, Houston, TX.

[2] To whom correspondence should be addressed.



0021-9517/92 $5.00

pirical; however, Wolf and Petersen (*33*) demonstrated that deactivation rate expressions could be derived from a reaction mechanism involving adsorption/desorption, surface reaction, and poisoning. More recently, Fuentes (*34*) and Corella *et al.* (*35*) have proposed deactivation models for systems in which reversible and partial deactivation occur, which involve the regeneration of poisoned sites; however, activation of initially inactive sites was not considered. Very recently, Agoretta *et al.* (*36*) have presented a kinetic model for activation–deactivation processes in solid catalysts, which considers activation of initially inactive sites as well as reversible and irreversible deactivation processes. A generalized activation–deactivation mechanism was assumed by these authors and it was used to determine rate expressions for site activation and deactivation. The activation–deactivation model was successfully fit to the experimental data of Fuentes *et al.* (*30*) for isomerization of *n*-butane over aluminum chloride/sulfonic acid resin catalysts.

Although catalyst activation is a somewhat common occurrence, no quantitative analyses of activation–deactivation behavior have been presented for carbon deposition from hydrocarbons on metal catalysts. In the case of carbon formation, Baker *et al.* (*5*) have indicated that the following steps are relevant.

(1) Hydrocarbons adsorb on the catalyst surface.

(2) The adsorbed hydrocarbon catalytically decomposes on the exposed surface of the catalyst particle leading to carbon laydown.

(3) Carbon deposits from the decomposition products dissolve into the metal particle.

(4) Carbon diffuses through the metal due to a temperature gradient established by the exothermic decomposition of the hydrocarbon.

(5) Carbon precipitates at the rear of the particle detaching the particle from the support and carrying it at the leading tip of the filament.

However, no attempts have been made to describe the reaction pathway in a quantitative manner. Several authors (*37–39*) attempted to explain experimental observations of carbon filament formation on the basis of thermodynamic arguments related to a gas-phase activity for carbon formation for the equilibrium of methane with hydrogen and graphite. Since, under the conditions of this study, no carbon deposition was observed from mixtures of $C_3H_6$ and $H_2$ in the absence of a catalyst, it was not appropriate to invoke thermodynamic arguments to relate the rate of deposition to gas-phase conditions. Previous studies also did not account for the activation/deactivation behavior which is important in carbon filament growth. Tibbetts *et al.* (*39*) proposed an adsorption–diffusion isotherm to predict the rate of growth of individual carbon filaments on Fe particles from $CH_4$; however, the model did not examine in detail the adsorption/desorption and surface reaction phenomena involved, nor were the effects of $H_2$ or catalyst activation explained. Bernardo and Lobo (*9*), Nishiyama and Tamai (*40*), and Cooper and Trimm (*11*) proposed more detailed reaction schemes consisting of adsorption and desorption, dehydrogenation and hydrogenation at the catalyst surface, carbon diffusion within the catalyst, and filament formation. However, no attempts to derive reaction rate expressions based on the proposed catalytic carbon formation schemes were made.

Since the fundamental heterogeneous processes which occur at the catalytic surface and the processes occurring in the catalyst bulk are of primary importance in carbon filament formation, these aspects must be considered in detail to explain the catalytic formation of carbon deposits. Thus, the first objective of this work was to propose a catalytic reaction sequence consisting of reaction steps at the catalyst surface and in the catalyst bulk, which was consistent with the generally accepted carbon filament formation mechanism, and with the experimental observations reported by McAllister and Wolf (*1*). The primary phenomena for which

the catalytic reaction sequence must account are catalyst activation and deactivation and the effects of $H_2$, which significantly increases the amount of carbon deposited for a given Ni loading and is important in the activation process, causing the rate of deposition to pass through a maximum. In addition, the pathway must explain the effects of the propylene concentration which alters the time lag of the activation behavior, but not the final total level of carbon deposited, and the linear dependence of carbon mass gain on Ni loading. Further, the proposed reaction steps must be consistent with the types of carbon deposits observed by SEM, which include individual carbon filaments and multiple filaments that are produced due to fragmentation of large catalyst particles. The second objective of this work was to derive rate expressions based on the proposed reaction pathway to predict qualitatively the trends observed in CCVI experiments. Finally, the kinetic model was compared with experimental data for Ni-catalyzed carbon deposition from $C_3H_6/H_2$ mixtures at varied gas-phase concentrations and temperatures to demonstrate quantitatively the agreement of theoretical calculations and experimental data and to determine values for the model parameters at varied conditions.

## 2. ACTIVATION–DEACTIVATION MODEL FOR CATALYTIC CARBON DEPOSITION

A reaction pathway consistent with the conditions and the carbon filament formation mechanism discussed in Section 1 follows.

*2.1. Reaction sequence.* The adsorption of the reactant from the gas phase on active site is

$$A + S_a \underset{k_{-1}}{\overset{k_1}{\rightleftharpoons}} [A \cdot S_a]. \qquad (1)$$

Here, $A$ corresponds to the parent hydrocarbon, $S_a$ is an active site for carbon deposition, and $[A \cdot S_a]$ is the adsorbed form of $A$ on $S_a$. Adsorption of the hydrocarbon is followed by a dehydrogenation reaction involving other active sites to form an adsorbed species, $H \cdot S_a$, and a carbonaceous precursor, $C \cdot S_a$:

$$[A \cdot S_a] + nS_a \underset{k_{-2}}{\overset{k_2}{\rightleftharpoons}} [C \cdot S_a] + n[H \cdot S_a]. \qquad (2)$$

Reaction (2) may involve several steps as additional hydrogen atoms are abstracted from the molecule. The coefficient $n$ will depend on the detailed mechanism of the dehydrogenation reaction and the nature of the adsorbed species. However, to simplify the model developed here, $n$ was specified as one and was not used as an adjustable parameter. At this point, at least three physically meaningful and realistic paths involving $[C \cdot S_a]$ can be proposed. The first is bulk diffusion of carbon through the active catalyst particle and deposition of $C$ at the opposite end, which is consistent with the filamentous carbon deposits reported by numerous other authors (*1–3, 37, 38, 41–44*). This process is likely to occur in small catalyst particles in which the diffusion path is relatively small. The actual mechanism of carbon diffusion and deposition at the back of the particle is a complex process and its driving force is not completely understood. Important to this analysis is the fact that carbon diffuses away from the reaction surface, which results in the regeneration of the active site and the formation of a carbon filament. While obviously not an elementary reaction step, this process is represented as

$$[C \cdot S_a] \underset{k_{-3}}{\overset{k_3}{\rightleftharpoons}} C + S_a. \qquad (3)$$

A second, competing pathway results in the poisoning of active sites corresponding to the deactivation of active sites, $S_a$, via encapsulation by carbon which has been observed in filament growth (*6, 41*). The deactivation,

$$[C \cdot S_a] \overset{k_4}{\rightarrow} P, \qquad (4)$$

is the usual form for catalyst deactivation by surface blockage (*33*). Here, $P$ is an irre-

versibly poisoned site no longer capable of catalyzing reactions.

Another pathway arises when carbon migrates from the top catalyst layer to the sublayer which was previously blocked. This process is likely to occur in large catalyst particles or on metal foils and leads to the formation of new active sites or activation of the catalyst as observed experimentally (*1*). This pathway is represented by

$$[C \cdot S_a] + S_i \underset{k_{-5}}{\overset{k_5}{\rightleftharpoons}} S_a + [C \cdot S_i], \quad (5)$$

where $S_i$ is a blocked, inactive site, and $[C \cdot S_i]$ is an unblocked inactive site occupied by $C$. The physical phenomenon is that of the catalytic particle being detached from the inactive site, while depositing the carbon on the underlying layer of catalyst. Once the inactive site has been exposed, it may be activated if $C \cdot S_i$, the adsorbed carbonaceous precursor, is displaced from its surface. Although several pathways which could lead to dissociation of $C$ from $S_i$ are conceivable, one realistic path is the hydrogenation of $C$ by reaction with a neighboring adsorbed species according to

$$[C \cdot S_i] + [H \cdot S_a] \underset{k_{-6}}{\overset{k_6}{\rightleftharpoons}} [B \cdot S_a] + S_a, \quad (6)$$

where $B$ is the hydrogenation product which will eventually desorb. Although other reactions can be proposed in place of reaction (6), it is necessary that site activation involve both $[C \cdot S_i]$ and $[H \cdot S_a]$ to concur with experimental results. For the case of catalytic carbon deposition from propylene in the presence of $H_2$, $H \cdot S_a$ corresponds to adsorbed $H_2$, and $B$ corresponds to $CH_4$ or $C_2H_4$, which were the primary gas-phase products observed (*1*). Reaction steps (5) and (6) represent the mechanism by which catalyst particles too large to form individual carbon filaments are fragmented to many smaller particles capable of catalyzing filament growth. Alternatively, these steps could also represent the gradual detachment of small particles from the support and thereby account for the activation period observed by Baker *et al.* (*5*) for carbon filament growth from 30-nm particles in which fragmentation did not occur.

Finally, the adsorption and desorption of $H$ and $B$ from active sites must be included:

$$[H \cdot S_a] \underset{k_{-7}}{\overset{k_7}{\rightleftharpoons}} H + S_a \quad (7)$$

$$[B \cdot S_a] \underset{k_{-8}}{\overset{k_8}{\rightleftharpoons}} B + S_a. \quad (8)$$

The above reaction sequence accounts for the primary phenomena involved in the catalytic formation of carbon deposits including adsorption and desorption of a parent hydrocarbon, reaction at the catalytic surface (Eq. (2)), transport of carbon away from the active faces of the catalytic particles (Eqs. (3) and (5)), precipitation of carbon to form filaments (Eq. (3)), deactivation of catalytic particles by carbon encapsulation (Eq. (4)), exposure of inactive catalytic sites by fragmentation of large catalytic particles (Eq. (5)), and activation of the exposed inactive sites by hydrogen (Eq. (6)). The analysis and results which follow demonstrate the implications of the operating conditions and site distributions on predicted catalytic carbon deposition and the relation to experimental observations. In addition, the reaction model has been fit to experimental data to quantitatively compare calculated results with experimental data for Ni-catalyzed carbon deposition from $C_3H_6/H_2$ mixtures.

*2.2. Derivation of rate expressions from proposed reaction steps.* An analysis similar to that used by Wolf and Petersen (*33*) for self-poisoning catalytic reactions was applied to derive expressions for the rates of formation of $C$, site poisoning, and site activation. Parallel to this work, Agoretta *et al.* (*36*) developed an activation–deactivation model based on assumed mechanisms for activation and deactivation using Langmuir–Hinshelwood rate expressions, while in the analysis presented here, rate expres-

sions are derived from the detailed reaction steps discussed in Section 2.1 to gain a more fundamental understanding of the important reactions and variables involved in catalytic carbon deposition. To simplify the analysis and to represent the physicochemical processes occurring, the following assumptions are made to derive the rate expressions:

(1) The total number of sites is constant (the sum of active, inactive, and poisoned sites).

(2) A pseudo-steady-state condition exists (i.e., rearrangement of species on the surface is much more rapid than the change rate of the number of active sites).

(3) Reaction (3) is rate controlling in the formation of $C$ and is irreversible.

(4) The poisoning or deactivation reaction, step (4), is irreversible.

(5) Reaction (6) is rate controlling for site activation and is irreversible.

Whereas the total number of *active* sites is not constant due to poisoning of sites and activation of inactive sites, the *total* number of sites, including active, inactive, and poisoned sites, is assumed constant. If the rates of adsorption and desorption are fast relative to the change rate of the number of active sites, then the surface concentrations of adsorbed species are near equilibrium, and the change in the number of active sites does not invalidate the pseudo-steady-state assumption. Assumption (5) is necessary for the model to agree with experimental results (*1*) which are strongly dependent on the hydrogen concentration. These assumptions lead to the following restrictions concerning the relative magnitudes of the rate constants:

$$k_{-3} \ll k_3 \ll k_2, k_{-2} \ll k_1, k_{-1} k_7, k_7 \quad (9)$$

$$k_4 < k_3 \quad (10)$$

and

$$k_{-6} \ll k_6 \ll k_5, k_{-5}. \quad (11)$$

If $k_4$ is not assumed smaller than $k_3$, active sites will be poisoned rapidly resulting in very little carbon deposition, which is an important case if carbon deposition is to be avoided. However, the purpose of this study is to investigate the case where significant deposition of carbon occurs.

If the total surface concentration of sites is $X_o$ (e.g., ($N_o$ sites)/cm$^2$), then

$$X_o = \sum_{i=1}^{8} X_i, \quad (12)$$

where for simplicity in notation, the following nomenclature is adopted:

$$X_1 = [S_a], \quad X_2 = [A \cdot S_a],$$
$$X_3 = [C \cdot S_a], \quad X_4 = [H \cdot S_a],$$
$$X_5 = [B \cdot S_a], \quad X_6 = [P],$$
$$X_7 = [S_i], \quad X_8 = [C \cdot S_i].$$

According to reaction (3) and subject to constraints (9) to (11), the reaction rate of carbon formation is written as

$$R = \frac{dC}{dt} = k_3 X_3, \quad (13)$$

where $R$ is the specific rate of carbon formation measured in molecules/cm$^2$/s. In addition, the rate of poisoning is

$$R_p = \frac{dX_6}{dt} = k_4 X_3, \quad (14)$$

where $R_p$ is the rate of poisoning measured in sites/cm$^2$/s, and the rate of activation of inactive sites, $R_a$, is

$$R_a = -\frac{dX_7}{dt} = k_6 X_4 X_8. \quad (15)$$

Under the conditions of (9) to (11), the pseudo-steady-state approximation is applied for the steps in the reaction sequence that are assumed to be in equilibrium for the adsorbed species $A$, $B$, and $H$ on active sites and the adsorbed species $C$ on inactive sites. Thus, the following equilibrium relationships are derived for $X_2$, $X_3$, $X_4$, $X_5$, and $X_8$.

$$X_2 = K_1[A]X_1 \quad (16)$$

$$X_3 = \frac{K_1 K_2}{K_7} \frac{[A]}{[H]} X_1 \quad (17)$$

$$X_4 = K_7[H]X_1 \tag{18}$$

$$X_5 = K_8[B]X_1 \tag{19}$$

$$X_8 = \frac{K_1K_2K_5}{K_7}\frac{[A]}{[H]}X_7, \tag{20}$$

where $K_i = k_i/k_{-i}$ is the equilibrium constant for the $i$th step, and the quantities $[A]$, $[B]$, and $[H]$ are the gas-phase concentrations of $A$, $B$, and $H$, respectively.

By substitution of Eqs. (16)–(20) into Eqs. (12)–(15), the following equations are obtained:

$$R = \frac{dC}{dt} = k_3\frac{K_1K_2}{K_7}\frac{[A]}{[H]}X_1 \tag{21}$$

$$R_p = \frac{dX_6}{dt} = k_4\frac{K_1K_2}{K_7}\frac{[A]}{[H]}X_1 \tag{22}$$

$$R_a = -\frac{dX_7}{dt} = k_6K_1K_2K_5[A]X_1X_7 \tag{23}$$

and

$$X_1 = \frac{X_o - X_6 - X_7}{\begin{array}{l}(1 + (K_1K_2K_5/K_7)([A]/[H])) \\ \hline (1 + K_1[A] \\ \quad + (K_1K_2/K_7)([A]/[H]) \\ \quad\quad + K_7[H] + K_8[B])\end{array}}. \tag{24}$$

Equation (24) differs from the self-poisoning case of Wolf and Petersen (*33*) by the presence of the $X_7$ term in the numerator, which results from the presence of blocked and occupied inactive sites.

To demonstrate the effects of different gas-phase conditions and site distributions on the behavior predicted by the proposed catalytic sequence, the site concentations are normalized by the total number of sites, and the rate constants in Eqs. (16)–(23) are grouped to obtain the forms

$$\frac{dc}{dt} = k_3'x_1 \tag{25}$$

$$\frac{dx_6}{dt} = k_4'x_1 \tag{26}$$

$$\frac{dx_7}{dt} = -k_6'x_1x_7 \tag{27}$$

$$x_2 + x_3 + x_4 + x_5 = k_1'x_1 \tag{28}$$

$$x_8 = k_2'x_7, \tag{29}$$

where $t$ is real time and the constants $k_3'$, $k_4'$, and $k_6'$ have units of inverse time. The normalized values $x_i$ and $c$ are defined as

$$x_i = \frac{X_i}{X_o} \quad \text{and} \quad c = \frac{C}{aX_o}, \tag{30}$$

where $x_i$ is the normalized surface concentration of type $i$ sites, $c$ is the number of $C$ atoms (or molecules) deposited normalized by the total number of sites, and $a$ is the surface area per unit substrate volume. Equations (16)–(18) and (20) are consolidated with Eq. (28) and substitution of (28) and (29) into (24) results in

$$x_1 = \frac{1 - x_6 - x_7(1 + k_2')}{(1 + k_1')}. \tag{31}$$

The constants in Eqs. (25)–(27) and (31) are defined as

$$k_3' = k_3\frac{K_1K_2}{aK_7}\frac{[A]}{[H]} \tag{32}$$

$$k_4' = k_4\frac{K_1K_2}{K_7}\frac{[A]}{[H]} \tag{33}$$

$$k_6' = k_6K_1K_2K_5[A]X_o \tag{34}$$

$$k_1' = K_1[A] + \frac{K_1K_2}{K_7}\frac{[A]}{[H]} + K_7[H] + K_8[B] \tag{35}$$

$$k_2' = \frac{K_1K_2K_5}{K_7}\frac{[A]}{[H]}. \tag{36}$$

The solution of Eqs. (25)–(27) and (31) was achieved by a Runge–Kutta fourth-order integration technique to solve the time-dependent equations with iterations required at each time step to converge upon a value of $x_1$. The following results were calculated to demonstrate the dependence of the catalytic carbon deposition model on changes in reaction conditions and the relation of these effects to the experimental observations reported by McAllister and Wolf

TABLE 1

Conditions and Parameter Settings for Catalytic Carbon Deposition Simulations

| Case No. | $[A]$ (mol/m$^3$) | $[H]$ (mol/m$^3$) | $x_{7_0}$ | $k_3'$ (h$^{-1}$) | $k_4'$ (h$^{-1}$) | $k_6'$ (h$^1$) |
|---|---|---|---|---|---|---|
| 1 | 1.0 | 1.0 | 0.9 | 1.0 | 0.1 | 0.5 |
| 2 | 0.5 | 1.0 | 0.9 | 0.5 | 0.05 | 0.25 |
| 3 | 0.25 | 1.0 | 0.9 | 0.25 | 0.025 | 0.125 |
| 4 | 2.0 | 1.0 | 0.9 | 2.0 | 0.2 | 1.0 |
| 5 | 1.0 | 0.5 | 0.9 | 2.0 | 0.2 | 0.5 |
| 6 | 1.0 | 0.25 | 0.9 | 4.0 | 0.4 | 0.5 |
| 7 | 1.0 | 0.1 | 0.9 | 10.0 | 1.0 | 0.5 |
| 8 | 1.0 | 2.0 | 0.9 | 0.5 | 0.05 | 0.5 |
| 9 | 1.0 | 1.0 | 0.5 | 1.0 | 0.1 | 0.5 |
| 10 | 1.0 | 1.0 | 0.3 | 1.0 | 0.1 | 0.5 |
| 11 | 1.0 | 1.0 | 0.95 | 1.0 | 0.1 | 0.5 |
| 12 | 1.0 | 1.0 | 0.99 | 1.0 | 0.1 | 0.5 |
| 13 | 1.0 | 1.0 | 0.8 | 1.0 | 0.1 | 0.5 |

(*1*) for Ni-catalyzed deposition of carbon from propylene/hydrogen mixtures.

## 3. RESULTS AND DISCUSSION

*3.1. Calculated results.* To reduce the number of adjustable parameters in solving Eqs. (25)–(27), $k_1'$ and $k_2'$ were assumed to be much less than one as would be the case at low surface coverages, and initial values were specified for $x_6$ and $x_7$. The rate expressions were integrated simultaneously to give the amount of $C$ formed, as well as the surface concentrations of active, poisoned, and inactive sites as functions of time. The effect of gas-phase composition was simulated by varying the relative values of $[A]$ and $[H]$. For purposes of comparison, a standard case was simulated for selected values of $k_3'$, $k_2'$, and $k_6'$ such that their relative magnitudes were $k_3' > k_6' > k_4'$ for $[A] = [H] = 1.0$ mol/m$^3$. Then, $[A]$ and $[H]$ were varied relative to one another and new values for the rate constants were determined relative to the standard values in accordance with the dependence of each parameter on $[A]$ and $[H]$ in Eqs. (32) to (34). With $k_1'$ and $k_2'$ considered negligible, and no sites initially poisoned, the only remaining independent variable was the initial concentration of inactive sites, $x_{7_0}$, which was set to 0.9 in the standard case. Table 1 lists the cases for which calculations were made and the values of $k_3'$, $k_4'$, and $k_6'$ used for different values of $[A]$ and $[H]$. The units of time for the results presented depend on the units of the rate constants which were specified as per hour; thus the units of time were hours. However, the actual time scale for the results shown in Figs. 1 to 4 was not necessarily realistic due to the arbitrary selection of the standard case parameters. These rate constant values and their limits were selected for comparison of the relative effects of operating variables and do not correspond directly to the time scales of the experiments conducted. However, the units of both rate constants and time can be scaled appropriately to fit experimental observations.

The solution of the standard case is displayed in Fig. 1, which shows the variation in the concentration of catalytic sites between active, inactive, and poisoned sites. For the standard case, the surface concentration of inactive sites ($x_7$) declined at a high rate initially, but the rate of disappearance decreased as time proceeded and a minimum value, which was slightly above zero because not all the initially inactive sites were activated, was approached. The concentration of deactivated sites ($x_6$) increased monotonically and leveled off after 60 h.

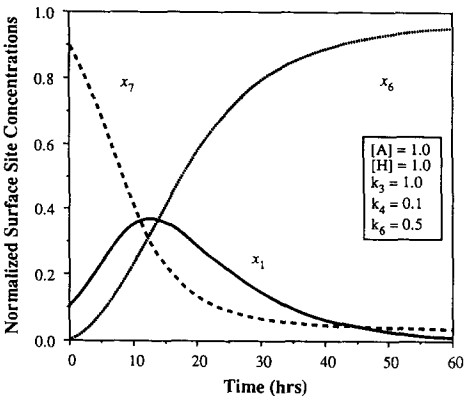


FIG. 1. Normalized surface concentrations of active, $x_1$, inactive, $x_7$, and poisoned sites, $x_6$, as functions of time for the standard case parameters.

Due to the combined effects of site activation and poisoning, the concentration of active sites ($x_1$) increased for a period of time, reached a maximum at the point where the rates of activation and poisoning were equal, and then declined as the rate of deactivation became greater than the rate of activation.

Shown in Fig. 2a are results for the normalized amount of $C$ formed as a function of time for different values of $[A]$, i.e., the gas-phase concentration of the parent hydrocarbon. As shown in Table 1 (cases 1 to 4), and according to Eqs. (32)–(34), changing $[A]$ resulted in linearly proportional shifts in $k_3'$, $k_4'$, and $k_6'$ (e.g., if $[A]$ doubled, $k_3'$, $k_4'$, and $k_6'$ doubled). As $[A]$ increased, the time period required to reach the maximum mass gain decreased and the shifting of the curves became less pronounced as a limiting condition was approached. The limiting condition was the case in which all sites were active initially, such that the maximum deposition rate occurred at the initial time. This limit was approached as the rate of activation increased so that most of the catalytic sites were activated in a very short period of time. Another feature of Fig. 2a is that, although the time over which $C$ was formed varied with $[A]$, the cumulative amount of $C$ formed at the point when no remaining active sites were constant. In physical terms, if $[A]$ increased, the rates of catalyst activation, poisoning, and carbon deposition all increased; however, the relative magnitudes of the rates of activation and deactivation with respect to the rate of deposition were not altered by changes in $[A]$. Thus, deposition occurred at higher rates but over shorter periods of time due to increased rates of activation and deactivation so that the total amount of carbon deposited was constant. The experimental results reported by McAllister and Wolf (*1*) exhibited qualitatively similar behavior to the calculated results of Fig. 2a, including the shortened deposition time with increased propylene concentration and the final level of carbon deposition which was nearly independent of the propylene concentration. However, the calculated results did not become completely independent of $[A]$ as observed experimentally (*1*), where above 3% propylene, a sharp transition to a regime of propylene concentration-independent carbon deposition was observed.

In addition to the amount of $C$ formed in Fig. 2a, the concentration of unoccupied active sites and the rate of formation of $C$ are shown in Figs. 2b and 2c. In Fig. 2b, the concentration of active sites, $x_1$, passed through a maximum and as $[A]$ increased, the time of maximum $x_1$ shifted toward the origin, which resulted in the S-shaped curves of Fig. 2a. The maximum in $x_1$ occurred because initially the rate of activation was greater than the rate of poisoning, but as time proceeded a point was reached at which the rate of activation became less than the rate of poisoning and $x_1$ declined. Although the time of maximum $x_1$ shifted, its magnitude was not affected. The rate of formation of $C$ was obtained by multiplying $x_1$ by $k_3'$, and the rate of formation of $C$ versus time for different values of $[A]$ is shown in Fig. 2c. Since a maximum in $x_1$ occurred, a maximum in the rate of generation of $C$ was present as well. In Fig. 2c, it is shown that for high values of $[A]$, the maximum occurred near the origin. But, as

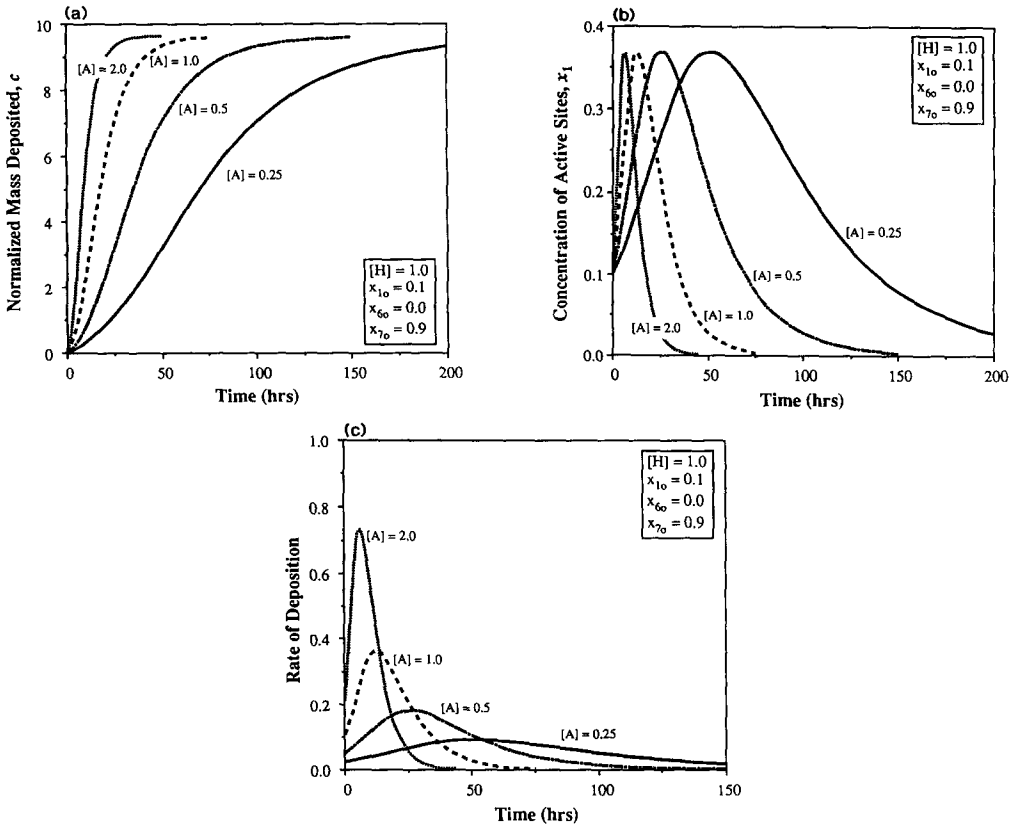


FIG. 2. The effects of the gas-phase hydrocarbon concentration on catalytic carbon deposition: (a) mass of carbon deposited, (b) surface concentration of active sites, and (c) the rate of carbon deposition.

[*A*] decreased the maximum decreased in magnitude and shifted to longer times. Although the magnitude of each maximum was different, the area under each curve, which yielded the same final amount of *C* formed as shown in Fig. 2a, was constant. The simulated rate behavior was similar to that reported by McAllister and Wolf (*1*), where the maximum rate was increased and shifted toward the origin as the propylene concentration increased to the point at which deposition became independent of changes in propylene concentration.

The effects of varying [*H*], which corresponds to varying the gas-phase hydrogen concentration, on the formation of *C* were evaluated and the results are shown in Figs. 3a and 3b. As with the effects of the reactant concentration, the calculated results displayed in Fig. 3 for various values of [*H*] follow the trend exhibited by experimental results (*1*), which showed the effects of hydrogen on Ni-catalyzed carbon deposition from propylene. Figure 3a shows the cumulative amount of *C* formed versus the dimensionless time for several different values of [*H*]. At low values of [*H*], rapid deactivation occurred and relatively little *C* formed. As [*H*] increased, the levels of *C* formed increased and the time over which formation of *C* occurred was extended; as [*H*] increased, the deactivation became more gradual. The experimental results of McAllister and Wolf (*1*) illustrate that as the $H_2$ concentration increased, the mass of carbon deposited increased significantly, the deposition occurred over longer periods of time, and the deactivation became more

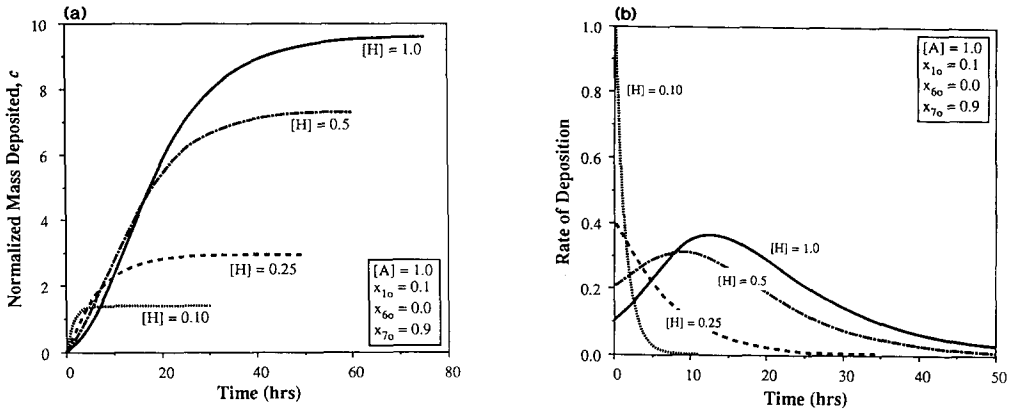


FIG. 3. The effects of the gas-phase hydrocarbon concentration on catalytic carbon deposition: (a) mass of carbon deposited and (b) the rate of carbon deposition.

gradual in a manner qualitatively similar to the results predicted by the model.

The rate of formation of $C$ is shown in Fig. 3b and in this graph the initial rate of formation of $C$ decreased with $[H]$. At values of $[H]$ less than 0.25, the initial rate of deposition was the maximum rate calculated and the rate declined rapidly to zero. As $[H]$ increased above 0.25, the initial rate decreased, but more importantly the rate of formation of $C$ did not decline monotonically but increased for a period of time, reached a maximum, and subsequently declined. The time at which this maximum was calculated to occur, shifted to slightly longer times as $[H]$ increased. Experimentally measured carbon deposition rates for different $H_2$ concentrations (*1*) exhibited similar behavior. At 0.0% $H_2$ feed concentration, the rate declined monotonically, but as the hydrogen concentration increased, the rates passed through a maximum which increased in magnitude as the $H_2$ content increased.

The calculated results shown in Fig. 3 can be explained in terms of the relative rates of formation of $C$, active site poisoning, site activation, and their respective variations with $[H]$. By definition, $k_3'$ and $k_4'$ are inversely proportional to $[H]$ while $k_6'$ is independent of $[H]$. Thus, at low values of $[H]$, $k_3'$ and $k_4'$ were large, which resulted in a high initial deposition rate and a high rate of poisoning. When $[H]$ increased, the rate constants for formation of $C$ and poisoning decreased proportionally while the rate constant for activation remained constant. Thus, a larger number of sites became activated because the rate of poisoning was reduced and consequently at a certain concentration of $H$, the rate of activation became greater than the rate of deactivation and a maximum in the rate of formation of $C$ occurred.

The remaining independent parameter was the initial fraction of inactive sites, $x_{7_0}$. The specification of this value set the initial distribution of sites between active and inactive. Small values of $x_{7_0}$ could correspond to a highly dispersed catalyst with most of the sites at the surface, while high values could represent larger catalyst particles with more sites contained in the bulk which were unable to catalyze reactions initially. A large initial fraction of inactive sites might occur even for a highly dispersed catalyst if the particle/support interaction is sufficiently strong to inhibit carbon filament formation. In this case, the activation process would correspond to the gradual detachment of particles from the support, which would result in an activation period as well. Figure 4 demonstrates the effects of different values of $x_{7_0}$ on catalytic carbon deposition. In general, as the fraction of inactive sites in-

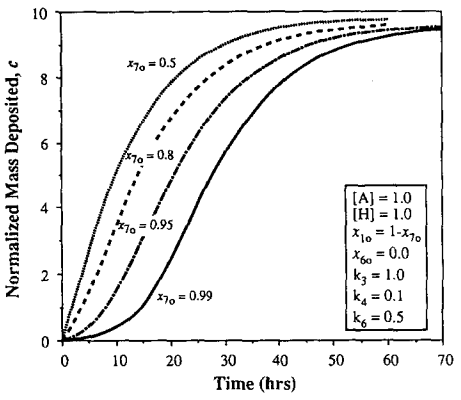


FIG. 4. The effects of the fraction of initially inactive sites on the mass of carbon deposited.

creased, the carbon deposition curves shifted to longer times because longer times were required to activate the sites. The shifting of the curves was minimal below $x_{7_0}$ = 0.5, but became increasingly significant as $x_{7_0}$ approached one.

*3.2. Optimized fit of reaction model to experimental data.* To determine if the proposed catalytic sequence and subsequent analysis could quantitatively predict experimental results for Ni-catalyzed carbon deposition from mixtures of propylene and hydrogen, calculated results were fit to the experimental data reported elsewhere (*1*). The fit to experimental data was obtained via a parameter optimization algorithm which systematically manipulated the independent parameters until the error between the theoretical values and the experimental data was minimized. The model calculations were obtained by solving Eqs.(25)–(27) and (31) as before, with $k_1'$ and $k_2'$ assumed to be negligible; so four independent parameters, $k_3'$, $k_4'$, $k_6'$, and $x_{7_0}$ remained.

The calculated results indicated qualitatively that the model predicted correctly the relation between carbon deposition and propylene concentration at low concentration (1–3%) but not at high concentration (>7%). While additional steps could be introduced to cover the whole range of concentrations, the few available experimental results did not permit a realistic fine tuning of the parameters. Thus it was deemed more practical to obtain rate constants at the two different ranges of concentration where results were available. The first set of rate constants were obtained using an optimization algorithm to fit the model parameters to the results obtained at low propylene concentration, (1–3%, Fig. 5). In this case, a first-order dependence was assumed between the rates of carbon deposition, deactivation, and activation with respect to propylene (Eqs. (32)–(36)). The second set of rate constants was obtained at high propylene concentration, assuming that the above referred rates were independent of propylene concentration in accord with Eqs. (41)–(43) explained below. A similar optimization procedure but with varying hydrogen concentration was used to obtain the new constants (Fig. 6). The constants are a combination of several equilibrium and reaction constants and thus represent lumped phenomenological values rather than true elementary step rate constants. Nonetheless, the model does predict quantitatively the experimental results at the low and high concentration separately, but not throughout the entire range.

To make a direct comparison of experimental data with theoretical values, the cal-

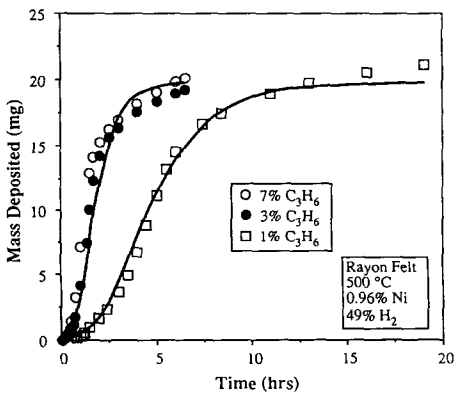


FIG. 5. Optimized fit of catalytic reaction model to experimental data for Ni-catalyzed carbon deposition at varied propylene concentrations.

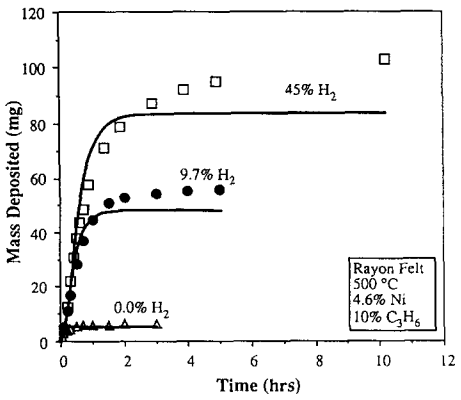


FIG. 6. Optimized fit of catalytic reaction model to experimental data for Ni-catalyzed carbon deposition at varied hydrogen feed concentrations.

culated values of the dimensionless quantity $c$ were converted to units of mass per unit substrate volume. According to the definition of $c$, the total number of sites per unit area, $X_0$, and the surface area per unit volume, $a$, of the substrate were required. As an approximation, $X_0$ was taken to be the ratio of the total number of Ni atoms loaded onto the substrate to the total surface area of the substrate, $a$, which was measured in BET experiments to be 525 $cm^{-1}$. The resulting value of $X_0$ was $9.8 \times 10^{16}$ sites/$cm^2/mg_{Ni}$. Thus, the following equation was used to convert $c$ to milligrams of carbon deposited:

$$M_c = 0.2046 m_{Ni} c \text{ (mg } C\text{)}, \quad (37)$$

where $M_c$ is the mass of carbon deposited, $m_{Ni}$ is the Ni loading in milligrams, and $c$ is the dimensionless mass gain from the model.

First, the model was fit to experimental data at 1–3% propylene concentrations and the results are displayed in Fig. 5. Experimental data are shown in Fig. 5 for propylene feed concentrations of 1, 3, and 7% for a rayon felt sample loaded with 0.96% Ni and infiltrated in the presence of 49% $H_2$ at 500°C. Two theoretical curves are presented in Fig. 5 for the conditions of 1 and 3% $C_3H_6$. The experimental data at these two conditions were fit simultaneously by manipulation of the parameters at 1% $C_3H_6$ and the calculation of the parameters for 3% relative to the 1% values according to the first-order dependence of the rate constants on $[A]$. The $C_3H_6$ concentration was tripled from 1 to 3%, and thus $k_3'$, $k_4'$, and $k_6'$ were tripled because of their linear dependence on the hydrocarbon concentration. However, $x_{7_0}$ was the same for both experiments since identical Ni loadings and substrate preparation techniques were used. The reaction model was able to fit the experimental data for these two sets of conditions quite well; however, when it was attempted to fit the data at 7% propylene as well, the fit was not as effective. Although the effect of increasing $[A]$ on the mass deposited vs time, as shown in Fig. 2a, decreased as $[A]$ increased, the model did not predict the abrupt transition to the regime of $C_3H_6$ concentration-independent carbon deposition as observed experimentally. According to the optimum fit of the model to the data, for which the parameter values are shown in Table 2, nearly 98% of the Ni present was in an inactive state initially. Although dispersion was not measured directly, SEM examination revealed that most of the Ni present on the surface was contained in particles on the order of 1 $\mu$m while carbon filament growth occurred from 50-nm particles indicating a low initial dispersion of active Ni particles. Thus, if the activation step was inhibited, a reduced amount of deposition would occur.

The $H_2$ concentration was of great importance in the Ni-catalyzed deposition of carbon from propylene. Since the results at different $H_2$ concentration were obtained at high propylene concentration in which the previous constants were not applicable, a new set of constants was obtained. Thus, utilizing the optimization procedure, the reaction model was fit to experimental data for catalytic carbon deposition at 0.0, 9.7, and 45% $H_2$ and 4.6% Ni on a rayon felt at 500°C and ~10% $C_3H_6$ in Fig. 6. As shown in Fig. 5, carbon deposition above 3% $C_3H_6$

TABLE 2

Optimum Parameters from Fit of Activation–Deactivation Model to Experimental Results

| Experiment | % $C_3H_6$ | % $H_2$ | % Ni Loading | $T$ (°C) | $x_{7_0}$ | $k_3'$ ($h^{-1}$) | $k_4'$ ($h^{-1}$) | $k_6'$ ($h^{-1}$) |
|---|---|---|---|---|---|---|---|---|
| 1 | 1.0 | 49.0 | 0.96 | 500 | 0.977 | 319.7 | 0.465 | 2.633 |
| 2 | 3.0 | 49.0 | 0.96 | 500 | 0.977 | 959.1 | 1.395 | 7.899 |
| 3 | 10.0 | 0.0 | 4.6 | 500 | 0.947 | — | — | 23.9 |
| 4 | 10.0 | 9.7 | 4.6 | 500 | 0.947 | 1418 | 2.48 | 23.9 |
| 5 | 10.0 | 45.0 | 4.6 | 500 | 0.947 | 305.7 | 0.535 | 23.9 |

becomes independent of the $C_3H_6$ concentration. Thus, Eqs. (21)–(23) were modified to be consistent with this fact and thus become

$$R = \frac{dc}{dt} = k_3 \frac{K_1K_2}{aK_7} \frac{X_1}{[H]} \tag{38}$$

$$R_p = \frac{dX_6}{dt} = k_4 \frac{K_1K_2}{K_7} \frac{X_1}{[H]} \tag{39}$$

$$R_a = -\frac{dX_7}{dt} k_6K_1K_2K_5X_1X_7 \tag{40}$$

or in Eqs. (32), (33), and (34), $k_3'$, $k_4'$, and $k_6'$ become independent of $[A]$:

$$k_3' = k_3 \frac{K_1K_2}{aK_7} \frac{1}{[H]} \tag{41}$$

$$k_4' = k_4 \frac{K_1K_2}{K_7} \frac{1}{[H]} \tag{42}$$

$$k_6' = k_6K_1K_2K_5X_0. \tag{43}$$

The optimal fit of the above constants to the data shown in Fig. 6 agreed reasonably well with all three data sets. At 9.7 and 45% $H_2$, the fit was good through the high deposition rate period during the first 2 h, but became less accurate as the model predicted a more rapid and complete deactivation than that which occurred experimentally. As a result, the model predictions were somewhat below the experimental data at longer times. For null hydrogen concentration in the feed, the model predicted almost instantaneous deposition to the maximum level, which was faster than observed experimentally, but the total amount of carbon deposited after a few minutes agreed well with experiments. The discrepancy in the initial period could be due to the experimental procedure in which propylene was introduced into the thermogravimetric apparatus at time zero. Because of the large volume enclosed by the chamber, there was a time lag before the $C_3H_6$ concentration reached its feed concentration at the substrate location.

The experimental conditions and the optimum model parameters determined for the varied propylene and hydrogen concentration experiments are given in Table 2. Although a 4.6% Ni loading was used in experiments 3, 4, and 5 as compared to 0.96% in experiments 1 and 2, the fractions of initially inactive sites obtained from the parameter optimizations were similar for both Ni loadings. According to the model fit, less than 6% of the catalytic material was active initially. The relative values of the constants $k_3'$, $k_4'$, and $k_6'$ were consistent with $k_3' > k_6' > k_4'$ in all cases. However, experiments 3, 4, and 5, conducted at 10% propylene, could not be fit simultaneously with experiments 1 and 2 at 1 and 3% $C_3H_6$ as indicated in the preceding discussion.

In previous work (*1*), it was shown that catalytic carbon deposition was affected by changes in temperature and the rate of deposition exhibited a complex dependence on temperature. To better understand the effects of temperature on catalytic carbon deposition, the catalytic model was fit to experimental data at various temperatures (*1*). The data at each temperature were fit independently to determine values for the parameters at each temperature and the results

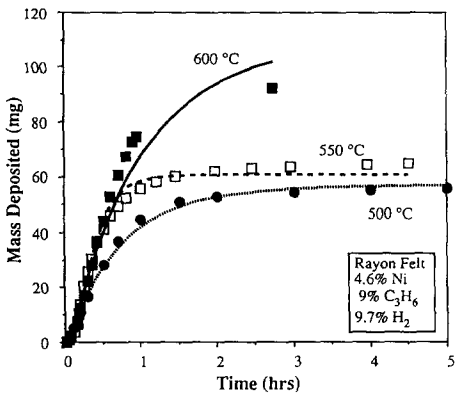


FIG. 7. Optimized fit of catalytic reaction model to experimental data for Ni-catalyzed carbon deposition at varied deposition temperatures.

are shown in Fig. 7. The agreement of the model with the data at 500°C was excellent, at 550°C the agreement was reasonably good, and at 600°C the model fit the experimental data initially, but overestimated the mass deposited at longer times. Catalytic carbon deposition at 600°C was so extensive that other factors such as diffusional limitations might have affected the mass gain of the substrate. The kinetic parameters obtained from the optimization are shown in an Arrhenius plot in Fig. 8. The rate constants for carbon deposition and catalyst deactivation passed through a maximum as the temperature was raised from 500 to 600°C, while the rate constant for activation exhibited a minimum in this temperature range. Clearly, the rate constants did not follow an Arrhenius temperature dependence, which indicated that the values determined from the fit to experimental data did not represent elementary reaction steps, but rather a lumped sequence of steps each with its own activation energy. However, the rate constants for deposition and deactivation did follow the trend of the experimental deposition rates reported by McAllister and Wolf (*1*). Due to the decrease in agreement between theory and experiment as temperature increased, and since the parameter optimization at each temperature was obtained from only one set of conditions, these parameters and the temperature dependence shown in Fig. 8 cannot be considered definitive. Obviously, the effects of temperature on catalytic carbon deposition are more complex than represented by the model and additional experiments and refinement of the proposed reaction steps are needed to describe better the effects of this variable.

## 4. CONCLUSIONS

To summarize the findings of the work presented here, the following conclusions are drawn:

(1) A sequence of reaction steps which corresponds to the fundamental phenomena of adsorption/desorption, catalyst activation and deactivation, surface reactions, and carbon diffusion and precipitation involved in catalytic deposition of carbon from hydrocarbons is proposed.

(2) Rate expressions for carbon deposition, catalytic site activation, and site poisoning derived from the reaction sequence, when integrated, yield results which exhibit trends qualitatively similar to experimental data for Ni-catalyzed carbon deposition from propylene/hydrogen mixtures.

(3) Increasing the $H_2$ concentration decreases the rates of deposition and poison-

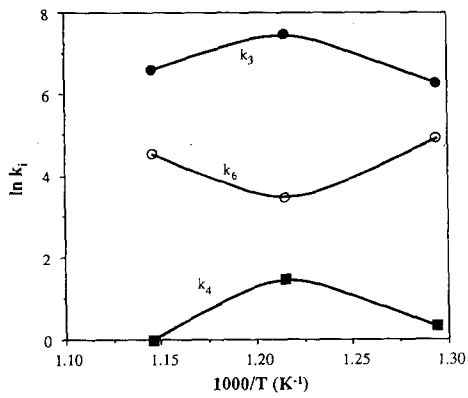


FIG. 8. Arrhenius plot of lumped rate constants for catalytic carbon deposition, $k_3$, site deactivation, $k_4$, and site activation, $k_6$, obtained from parameter optimization at 500, 550, and 600°C.

ing but does not affect the rate of site activation. Thus, higher $H_2$ concentrations lead to lower initial deposition rates, but the total level of deposition increases because of reduced deactivation rates.

(4) The hydrocarbon concentration affects the rates of activation, poisoning, and deposition in the same manner, so that the ultimate level of deposition is independent of the hydrocarbon concentration. However, as the hydrocarbon concentration increases, the time over which deposition occurs decreases due to an increased rate of deactivation.

(5) The activation–deactivation–deposition model effectively accounts for the effects of $H_2$ on carbon deposition for $H_2$ feed concentrations from 0.0 to 45%, and the effects of $C_3H_6$ concentration are fit well up to 3% propylene where carbon deposition becomes independent of $C_3H_6$. Optimized fits of the model to experimental data at varied temperatures show that the model agrees well with data at temperatures of 500 and 550°C, but the agreement is less satisfactory at 600°C.

In summary, the activation–deactivation–carbon deposition model proposed in this work incorporates the fundamental, heterogeneous steps involved in catalytic carbon deposition and consequently, represents well the trends observed experimentally for catalytic carbon deposition. The limitations of the model include the prediction of a gradual transition to propylene-independent carbon deposition rather than the observed sharp transition and the less satisfactory fit to data above 550°C. Several simplifying assumptions, which if treated differently may improve the agreement of theory and experiment, were made. For instance, low surface coverage which will become less valid as the hydrocarbon concentration increases was assumed. Also, the orders of certain reaction steps could be different from those assumed. Modifications to these assumptions could improve the agreement between theory and experiment, but additional parameters would be introduced as well. In this analysis, we attempted to limit the number of adjustable parameters so that the physical significance was not obscured. Thus, the model and assumptions presented in this work correspond well qualitatively, and under most conditions examined, quantitatively, to experimental observations.

## 5. NOTATION

| | |
|---|---|
| $a$ | surface area per unit volume |
| $A$ | hydrocarbon reactant |
| $[A]$ | gas-phase hydrocarbon concentration |
| $[A \cdot S_a]$ | hydrocarbon adsorbed on an active site |
| $B$ | gaseous hydrogenation product |
| $[B]$ | gas-phase concentration of B |
| $[B \cdot S_a]$ | adsorbed hydrogenation product |
| $c$ | carbon atoms (or molecules) deposited per site |
| $C$ | carbon deposit |
| $[C \cdot S_a]$ | carbon deposit associated with an active site |
| $[C \cdot S_i]$ | carbon deposit associated with an initially inactive site |
| $H$ | hydrogen |
| $[H]$ | gas-phase hydrogen concentration |
| $[H \cdot S_a]$ | hydrogen adsorbed on an active site |
| $k_i$ | rate constant for forward reaction step |
| $k_{-i}$ | rate constant for reverse reaction step |
| $k_3'$ | lumped rate constant for rate of carbon deposition |
| $k_4'$ | lumped rate constant for rate of poisoning |
| $k_6'$ | lumped rate constant for rate of site activation |
| $k_1'$ | lumped constant for coverage of active sites |
| $k_2'$ | lumped constant for coverage of initially inactive sites |
| $K_i$ | equilibrium constant for reaction $i$ |
| $P$ | poisoned sites |
| $R$ | rate of carbon deposition |
| $R_a$ | rate of site activation |

$R_p$ rate of site poisoning or deactivation
$S_a$ active site
$S_i$ initially inactive site
$t$ time
$x_i$ surface concentration of type $i$ sites normalized by total surface concentration of sites
$X_i$ surface concentration of type i sites
$X_o$ total surface concentration including all types of sites (constant)

## REFERENCES


1. McAllister, P., and Wolf, E. E., *Carbon* **30,** 189 (1992).
2. Baker, R. T. K., *Carbon* **27** (3), 315 (1989).
3. Baker, R. T. K., *Catal. Rev. Sci. Eng.* **19**(2), 161 (1979).
4. Tesner, P. A., Robinovich, E. Y., Rafalkes, I. S., and Arefieva, E. F., *Carbon* **8,** 435 (1970).
5. Baker, R. T. K., Barber, M. A., Harris, P. S., Feates, F. S., and Waite, R. J., *J. Catal.* **26,** 51 (1972).
6. Baker, R. T. K., Harris, P. S., Thomas, R. B., and Waite, R. J., *J. Catal.* **30,** 86 (1973).
7. Bernardo, C., and Lobo, L. S., *Carbon* **14,** 287 (1976).
8. Nishiyama, Y., and Tamai, Y., *J. Catal.* **33,** 98 (1974).
9. Bernardo, C. A., and Lobo, L. S., *J. Catal.* **37,** 267 (1975).
10. Keep, C. W., Baker, R. T. K., and France, J. A., *J. Catal.* **47,** 232 (1977).
11. Cooper, B. J., and Trimm, D.L., *J. Catal.* **62,** 35 (1980).
12. Baker, R. T. K., and Chludzinski, J. J., Jr., *J. Catal.* **64,** 464 (1980).
13. Baker, R. T. K., Alonzo, J. R., Dumesic, J. A., and Yates, D. J. C., *J. Catal.* **77,** 74 (1982).
14. Olazar, M., Aguayo, A. T., Arandes, J. M., and Bilbao, J., *Ind. Eng. Chem. Res.* **28,** 1752 (1989).
15. McDaniel, M. P., and Johnson, M. M., *J. Catal.* **101,** 446 (1986).
16. Cunningham, J., Al-Sayyed, G. H., Cronin, J. A., Fierro, J. L. G., Healy, C., Hirschwald, W., Ilyas, M., and Tobin, J. P., *J. Catal.* **102,** 160 (1986).
17. Hicks, R. F., and Bell, A. T., *J. Catal.* **90,** 205 (1984).
18. Nix, R. M., Judd, R. W., Lambert, R. M., Jennings, J. R., and Owen, G., *J. Catal.* **118,** 175 (1989).
19. Montes, M., Penneman De Bosscheyde, Ch., Hodnett, B. K., Delannay, F., Grange, P., and Delmon, B., *Appl. Catal.* **12,** 309 (1984).
20. Krebs, H. J., Bonzel, H. P., and Schwarting, W., *J. Catal.* **72,** 199 (1981).
21. Tau, L. M., and Bennett, C. O., *J. Catal.* **96,** 408 (1985).
22. Pijolat, M., Perrichon, V., and Bussiére, P., *J. Catal.* **107,** 82 (1987).
23. Bukur, D. B., Mukesh, D., and Patel, S. A., *Ind. Eng. Chem. Res.* **29,** 194 (1990).
24. Kuivila, C. S., Stair, P. C., and Butt, J. B., *J. Catal.* **118,** 299 (1989).
25. Jnioui, A., Eddouasse, M., Amariglio, A., Ehrhardt, J. J., Alnot, M., Lambert, J., and Amariglio, H., *J. Catal.* **106,** 144 (1987).
26. Kikuchi, E., Wada, H., Fujishiro, K., Chiba, T., and Morita, Y., *Int. Chem. Eng.* **24**(4), 710 (1984).
27. Perti, D., and Kabel, R. L., *AIChE J.* **31**(9), 1420 (1985).
28. Laine, J., Brito, J., Gallardo, J., and Severino, F., *J. Catal.* **91,** 64 (1985).
29. Noelke, C. J., and Rase, H. F., *Ind. Eng. Chem. Prod. Res. Dev.* **18**(4), 325 (1979).
30. Fuentes, G. A., Boegel, J. V., and Gates, B. C., *J. Catal.* **78,** 436 (1982).
31. Amariglio, A., Lakhdar, M., and Amariglio, H., *J. Catal.* **81,** 247 (1983).
32. Forzatti, P., Buzzi-Ferraris, G., Morbidelli, M., and Carrá, S., *Int. Chem. Eng.* **24** (1), 60 (1984).
33. Wolf, E. E., and Petersen, E. E., *J. Catal.* **47,** 28 (1977).
34. Fuentes, G. A., *Appl. Catal.* **15,** 33 (1985).
35. Corella, J., Adanez, J., and Monzón, A., *Ind. Eng. Chem. Res.* **27,** 375 (1988).
36. Agorreta, E. L., Peña, J. A., Santamaria, J., and Monzón, A., *Ind. Eng. Chem. Res.* **30,** 111 (1991).
37. Alstrup, I., *J. Catal.* **109,** 241 (1988).
38. Bianchini, E. C., and Lund, C. R. F., *J. Catal.* **117,** 455 (1989).
39. Tibbetts, G. G., Devour, M. G., and Rodda, E. J., *Carbon* **25**(3), 367 (1987).
40. Nishiyama, Y., and Tamai, Y., *J. Catal.* **45,** 1 (1976).
41. Downs, W. B., and Baker, R. T. K., *in* "Proceedings, 20th Biennial Conference on Carbon, Santa Barbara, CA," p. 318, 1991.
42. Rostrup-Nielsen, J., and Trimm, D. L., *J. Catal.* **48,** 155 (1977).
43. Trimm, D. L., *Catal. Rev. Sci Eng.* **16**(2), 155 (1977).
44. Rostrup-Nielsen, J. R., *in* "Catalysis: Science and Technology" (J. R. Anderson and M. Boudart, Eds.), Vol. 5, pp. 73–95. Springer-Verlag, Berlin, 1984.